

# FORESTCAST: FORECASTING DEFORESTATION RISK AT SCALE WITH DEEP LEARNING

**Matthew Overlan \***      **Charlotte Stanton**      **Maxim Neumann**      **Arianna Manzini**

**Julia Haas**      **Michelangelo Conserva**      **Mélanie Rey**      **Kira Prabhu**      **Youngin Shin**

**Kuan Lu**      **Drew Purves**

## ABSTRACT

Deforestation is a major threat to biodiversity and the stability of the climate. Current monitoring solutions provide reactive alerts only after deforestation has occurred, rendering them inadequate for prevention. Proactive deforestation prevention necessitates forecasting at-risk areas, however, previous forecasting efforts have been constrained by their reliance on simple statistical models and limited feature sets. This paper introduces the ForestCast Southeast Asia dataset, the first publicly available dataset dedicated to training deep learning models for the task of deforestation risk forecasting. We benchmark several deep learning models from the literature, as well as a Random Forest Decision Tree model, and find that the deep learning models perform the best. Furthermore, we test the relative importance of three classes of input data: satellite imagery, derived feature layers such as slope and distance to roads, and change history, an image summarizing past deforestation. Surprisingly, we find that our best models can achieve equal results using only the change history as input. Lastly, we present a preliminary assessment of the ethics of using deforestation risk models in practice.

## 1 INTRODUCTION

Deforestation poses a critical threat to global biodiversity and climate stability, with total tropical primary forest loss in 2024 reaching 6.7 million hectares—equivalent to almost 18 football (soccer) fields of forest lost every minute (Weisse et al., 2024). This loss not only endangers countless species but also disrupts vital ecosystem services, including carbon sequestration and water regulation (Daily et al., 1997). Indeed, forests play an essential role in sustaining livelihoods, particularly in tropical regions where many communities depend on these ecosystems for their survival and economic prosperity (IPBES, 2019; Food and Agriculture Organization, 2014).

Much of the devastation inflicted on forests is driven by unsustainable business practices, including agricultural expansion, logging, and infrastructure development. These activities have drawn increasing scrutiny from investors (Holder, 2021) and regulators (Schröder, 2022) alike, prompting calls for improved environmental performance from companies across various sectors. The European Union Deforestation Regulation (EUDR, European Commission: Directorate-General for Environment (2023); European Union (2023)) exemplifies this shift, by curbing the import of products linked to deforestation and requiring companies to demonstrate compliance with sustainable sourcing practices. In turn, businesses are adapting to a landscape where environmental stewardship is no longer optional but a prerequisite for market participation.

To effectively navigate these changes, the ability to predict deforestation trends is paramount. Forecasting high-risk areas would enable companies to proactively manage their supply chains, mitigating potential disruptions and aligning their operations with sustainability goals. Such foresight would not only benefit corporations but also non-governmental organizations dedicated to conserva-

---

\*The authors wish to thank Michal Kazmierski, Chris Brown, Valerie Pasquarella, Alexis Boukouvalas, Sophia Alj, Maria Abi Raad, Ben Bariach, Dan Morris, Gena Gibson, Henry Glick, Andrew Wilcox, and Michael Marano for helpful discussions and other contributions to this work.

tion efforts. Equipping NGOs with predictive insights would empower them to target interventions more effectively, safeguarding forests before they fall victim to irreversible damage. Moreover, for indigenous peoples and local communities, predictive models could serve as tools for advocacy and empowerment. By providing early warnings of potential deforestation, forecasts could help communities mobilize and take action to protect their ancestral lands and resources.

Finally, deforestation risk forecasting can also enhance the integrity and effectiveness of conservation investments. Assessing the additionality of such investments - demonstrating that conservation outcomes would not have occurred without a given intervention — is a critical challenge. Predictive models like the one presented here can provide a baseline of likely deforestation in the absence of an intervention, allowing for a more robust evaluation of its potential impact. Notably, carbon credit standard-setting organizations have started integrating deforestation risk probabilities into their methodologies to provide a more rigorous framework for assessing the impact of avoided deforestation projects. This integration underscores the recognition of predictive modeling as an essential tool for increasing the credibility and effectiveness of conservation finance.

This manuscript explores the potential of deep learning to forecast deforestation risk, shifting from reactive monitoring to proactive prevention. To address the needs of governments, NGOs and actors in the private sector, we leverage large-scale satellite imagery and the latest computer vision AI models, to create a deforestation risk methodology that is:

- **Accurate**, in that the model predictions are at least as accurate as previous models, most of which rely only locally specific features such as roads and / or statistical (non deep learning) models. We demonstrate this by comparing our pure satellite model to a set of such models, using the same training and evaluation data, and the relative contribution of three classes of input features to better understand the drivers of model performance.
- **Trustworthy**, in that we compare the relative importance of three classes of input features to better understand the drivers of model performance, and we measure performance on two distinct sources of ground truth data. These novel evaluations strengthen trust that the final model is as accurate as it can be.
- **Consistent**, in that the same machine learning model, with the approach to training data, inputs, evaluation, can be used anywhere, allowing for meaningful comparisons across regions. We achieve this by using globally, satellite-derived training and inputs only.
- **Future Proof**, in that we can be confident that the model inputs will be refreshed in future years, allowing for updated calculations of risk, and meaningful comparison across years. Again the pure satellite approach achieves this, because the satellite-derived inputs are expected to be made available every year for the foreseeable future.
- **Scalable**, in that the methodology is sufficiently computationally efficient to run at high resolution over large regions, potentially all the way to global. We achieve this by using recent deep learning vision models that work tile-to-tile (i.e. take in a grid of pixels, and output a grid of pixels); and moreover we find that accurate predictions requires only a single tile of integers as input (the change history — see below)
- **Verifiable and Transparent**, in that the research community can repeat and build on our work. We achieve this by releasing the training and evaluation data used in this manuscript as a machine learning benchmark.

## 2 PRIOR WORK

Several previous works have considered the problem of deforestation risk forecasting, using a variety of methods and data sources. We survey several relevant machine learning-based works here, noting that there is an earlier literature based on other methods (Rosa et al., 2013). Together, these machine learning studies prove that it is sometimes possible to predict deforestation risk to a high accuracy at local scales. However, these methods do not meet the criteria listed above. Most studies rely on combinations of locally-tailored approaches to training data; and / or local specialized input features that are not available everywhere, and may quickly go out of date; and thus, are not consistent or future proof. Furthermore, most of the models have not released their training and input data, which hampers verifiability and transparency.

Our work is most similar to that of Ball et al. (2022) who used deforestation labels from Global Forest Change dataset from Global Forest Watch (GFW-GFC) (Hansen et al., 2013), and trained on the composite satellite images included in that dataset for two regions in the Peruvian Amazon. They evaluated several convolutional neural networks, achieving good results particularly with the 3D CNN. While Ball et al. uses globally available training and input data, it utilizes a model that is hard to scale to large regions (the Ball et al. model works tile-to-pixel, and hence requires a costly moving window approach to predict for large regions). Moreover, Ball et al. (or any other work) have not ablated input data to compare their relative importance, and they have not released their training dataset, making it hard to repeat or build on the work.

Engelmann & Toetzke (2023) also used deep convolutional models (UNet and ResUNet), although they used MAPBIOMAS data (Souza et al., 2020) for input and labels over the Brazilian Amazon, however they were unable to achieve good scores until coarsening the task to predict tile-level deforestation rates.

Another recent work leveraging a deep learning model is Goldman et al., which used Land Change Modeler (Eastman & Toledano, 2018) to predict labels from GFC using a suite of features including forest cover and forest loss from GFC, distance to roads, land cover, protected areas, concessions data, and more. The proprietary Land Change Modeler from Clark Labs is a software tool for modeling land cover change. It provides an interface for training models (such as Multi-layer Perceptron and logistic regression) to predict the probability of land cover transitions given explanatory variables provided by the user. The trained model can then be used to simulate future transition quantity and spatial distribution. They reported high accuracies for several areas in the Democratic Republic of Congo.

Works utilising statistical (non deep learning) models, include Jaffé et al. (2021), which used a Bayesian hierarchical spatial model to forecast deforestation in the Brazilian Amazon, using MAPBIOMAS data for labels and 20 input variables such as distance to urban areas, distance to roads, GDP, and forest edge density. Sales et al. (2017) used highly modified Generalized Linear Models (to account for spatial correlation, for example) to model deforestation in the Brazilian Amazon, using PRODES (National Institute For Space Research) data as labels and similar input features as above. Sboui et al. (2023) created their own deforestation labels for northern Sumatra, Indonesia using NDVI (which is derived from satellite data), and trained a random forest model based on variables such as distance to roads and rivers. van Stokkom et al. (2020) created their own deforestation labels for an area in Borneo, Indonesia using Sentinel 1 satellite data. They then found that gradient-boosted decision trees gave the best results on their data. [DWP — cover inputs of this last study]

Vieilledent et al. (2023) modeled deforestation risk over the entire tropics, the only prior work to our knowledge to do so. They used deforestation data from Vancutsem et al. (2021) as labels, and six input features such as distance to roads, etc. They trained three pixel-to-pixel models and found that their spatially-augmented logistic regression performed the best. [DWP — state model, was this deep learning? If so maybe put just under the two deep learning models listed above]

A final note is that at time of writing, the approach to deforestation risk modeling with the greatest uptake in practice, appears to be the Forest Loss Risk Index (FLRI) (Satelligence, 2022). This is a non-learned model, i.e. a heuristic, that assumes risk is linearly related to distance from previous deforestation in both space and time. The fact that the FLRI is currently the default choice for most practitioners suggests that machine-learning based approaches to deforestation risk have not yet matured to the point where they are sufficient to guide decision makers worldwide.

### 3 METHODS

#### 3.1 HISTORICAL DEFORESTATION DATASET

Despite these prior works, there is not yet a standard dataset and benchmark for predicting future deforestation. Consequently, recently released aggregated datasets for large geospatial model training such as FoMo-Bench (Bountos et al., 2023) and GEO-Bench (Lacoste et al., 2023) do not include any temporal forest datasets. We hope that by describing our dataset and releasing it publicly, it can become a resource that other researchers can use to accelerate progress on this important task.

Our dataset is designed to train deforestation risk forecasting models for fixed time intervals. The dataset and results here cover tropical Southeast Asia, but our methods and data sources are globally applicable.

### 3.1.1 LABELS

To create a historical deforestation dataset with both global spatial coverage and deep historical temporal coverage, we used algorithmically derived deforestation events as our ground truth labels. This bypasses the need for costly human annotation, at the possible expense of accuracy. We evaluate on two sources of target data made available to the community by others: the Global Forest Change dataset (Hansen et al., 2013), a widely used product which has been providing deforestation monitoring and alerts since 2012; and the Continuous Change Detection and Classification (CCDC) algorithm (Zhu & Woodcock, 2014).

The GFW-GFC annual change maps were produced by extracting a time series of spectral features from Landsat 7 imagery and then training a bagged decision tree classifier to classify pixels as changed or unchanged.

The CCDC algorithm operates on single-pixel time series and fits a variable number of breakpoints that best identify sharp changes in the luminance values of that time series. When applied to forested areas, it fairly reliably identifies forest to non-forest transitions. Our CCDC data were generated using Google Earth Engine’s `ee.Algorithms.TemporalSegmentation.Ccdc` algorithm over Landsat data from 2000-2023 (inclusive) (Gorelick et al., 2023). To create labels that can act as a prediction target, we created a mask indicating for every pixel whether a segment ended (as indicated by the `tEnd` band) during the forecast time interval.

Regardless of the source of target labels, we use the GFW-GFC dataset to mask out all non-forest areas, defined as pixels that were either non-forest prior to 2000 (`treecover2000` band  $< 25\%$ ) or have experienced a loss event before the start of the forecast time interval.

These two algorithms yield qualitatively and quantitatively different change masks, so it is important to acknowledge that the quality of any risk forecast is constrained by the quality of the associated training labels.

### 3.1.2 INPUT DATA

To predict these deforestation events, we constructed a historical deforestation dataset based on satellite time series features. This is in contrast to previous work on deforestation risk forecasting which uses static features derived from satellite imagery and other sources, such as proximity to roads, or composite satellite imagery, as described in section 2.

Our dataset includes several different sources, enabling us to compare the effectiveness of different input features. We include two sources of satellite imagery, one a dense time-series (containing all images within the year prior to the forecast date), and the other annual composites dating back to 2014. Satellite imagery is augmented with auxiliary data layers showing mostly static information, such as elevation, distance to roads, etc. The full list of auxiliary data sources is shown in Table 1.

Finally, we include a record of past change for each pixel showing how long ago in years that pixel was deforested, along with a binary mask showing which pixels have experienced deforestation. This change-history layer corresponds to the data source used for the segmentation label (GFW-GFC or CCDC).

All data were downloaded from the Earth Engine Data Catalog (Gorelick et al., 2017) except for GRIP and GWL which were downloaded from the GEE Community Catalog (Roy et al., 2024). All images were resampled to a resolution of 30m/pixel to match the resolution of the GFW-GFC labels.

### 3.1.3 TEMPORAL COVERAGE

To train our model, we constructed historical data by dividing the satellite imagery and other temporal data into several temporal shards. Each shard consists of all data sources from Table 1, Sentinel 2 imagery covering one year prior to the split data, and annual composite imagery from GFW going back to 2014. This is combined with label information for that year (Figure 1).

| Dataset  | Source                      | Description  |
|--|-----------------------------|--|
| Sentinel 2 L1C                                 | ESA                         | Multi-spectral satellite imagery (10m, 5-10 day revisit time)  |
| Global Forest Change                           | GFW                         | Historical deforestation (30m, annual), tree cover, permanent water, and annual Landsat composite images |
| CCDC   | Google                      | Historical land change   |
| World Database on Protected Areas              | UNEP-WCMC, Protected Planet | Protected area boundaries  |
| Gridded Population of the World                | NASA SEDAC                  | Population density   |
| SRTM Digital Elevation                         | NASA/CGIAR                  | Elevation above sea level in meters  |
| Oil Palm Plantation                            | Forest Data Partnership     | Palm plantation  |
| CloudScore+                                    | Google                      | Cloud mask   |
| Global Roads Inventory Project                 | GLOBIO                      | Roads  |
| Global Mangrove Distribution                   | ORNL DAAC                   | Mangroves & wetlands   |
| Global Wetland with Fine Classification System |                             | Wetlands   |

Table 1: Data sources included in the ForestCast dataset.

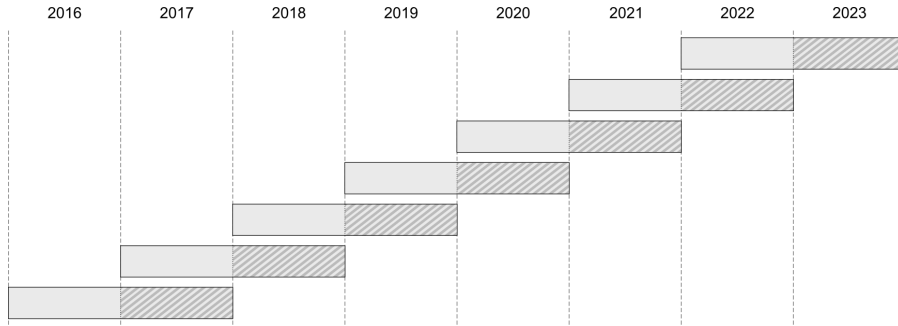


Figure 1: Dataset shards. Each temporal shard contains a year of satellite imagery and auxiliary data, plus deforestation labels for the following year (indicated by the shaded areas).

At training time we aggregate data from all shards prior to the year we wish to forecast. For example, if we wish to generate forecasts for 2023, we train the model on all shards from 2022 and before. In this way, we simulate the situation where a model will be trained on all available historical data up to the present moment and be used to forecast an interval starting at the present moment.

#### 3.1.4 SPATIAL COVERAGE

We constructed our dataset by first sampling many points over the forested areas of tropical South-east Asia (Figure 2), and then constructing training examples for each point.

To sample points, we first construct a covering grid of size  $7680\text{m}^2$ , which corresponds to  $256 \times 256$  pixels at 30m resolution. We remove grid cells that have no or nearly no forest cover, then randomly assign each cell to one of 8 classes, one for each dataset split, and one reserved for future



Figure 2: The study region covers UN-defined Southeast Asia bounded by the tropics.

| Year | Number of samples |
|------|-------------------|
| 2017 | 11052             |
| 2018 | 10889             |
| 2019 | 10829             |
| 2020 | 11057             |
| 2021 | 10969             |
| 2022 | 10970             |
| 2023 | 10896             |

Table 2: The number of samples in each dataset split.

splits. We then sample a tile of pixels for each grid cell assigned to a dataset split. This resulted in approximately 11,000 examples per split, as shown in Table 2

Each tile consists of a collection of 4D tensors with dimensions *time*, *height*, *width*, and *channels*, that can be ingested by deep learning models. All tiles have a pixel size of 30m and height and width of 7690m (256 pixels), but have varying time and channel dimensions based on the source dataset. Because deforestation happens to only a small fraction of pixels at any one time relative to the total area of forest, the dataset features heavy class imbalance, with an overall proportion of 0.65% of pixels labeled as deforestation.

### 3.2 MODELS

#### Random Forest Decision tree

We tested gradient-boosted decision trees using the Yggdrasil Decision Forests (YDF) library (Guillame-Bert et al., 2023). This is a pixel-wise model, operating on each pixel independently.

#### UNet3D

The UNet3D architecture is an extension of the U-Net convolutional architecture (Ronneberger et al., 2015) to handle temporal features. We follow the architecture used by Rustowicz et al. (2019). U-Net models employ successive stages of downsampling convolution, followed by successive stages of upsampling transposed convolution, all with residual connections between the down and up intermediate layers at each resolution.

#### U-TAE (U-Net with Lightweight Temporal Attention)

The U-TAE architecture (Garnot & Landrieu, 2021) was initially developed for crop segmentation, for which it was recently state of the art. It combines convolution for spatial processing with self attention for temporal processing. The self-attention collapses the temporal dimension at the bottom-most, or most coarse level of the U-Net. The architecture employs a simplified attention mechanism

that was shown to increase speed while sacrificing little to no performance (Garnot & Landrieu, 2020).

### TSViT (Temporal-Spatial Vision Transformer)

The TSViT model (Tarasiou et al., 2023) is an extension of the original vision transformer model (Dosovitskiy et al., 2020), which employ self-attention transformers applied to image patches to perform vision tasks. The TSViT model adapts the ViT architecture for satellite image time series by factorizing the transformer encoder into self-attention blocks that sequentially process the temporal and then spatial dimensions. It further introduces multiple learnable class tokens (one per class) and acquisition-time-specific temporal positional encodings to handle irregularly sampled data.

## 3.3 TRAINING

### 3.3.1 DATA PREPROCESSING

| Dataset   | Bands included  | Description  |
|---|---|--|
| Sentinel 2 L1C (Copernicus, 2025)                                   | B2 (Blue), B3 (Green), B4 (Red), B8 (NIR), B11 (SWIR) | Pixel values were log transformed via $\log_{10}(x+1)$ then each band normalized by its dataset mean and standard deviation. |
| Global Forest Change (Hansen et al., 2013)                          | treecover2000, lossyear, datamask                     | Construct a binary water mask from the datamask band.  |
| World Database on Protected Areas (UNEP-WCMC and IUCN, 2024)        | N/A   | Binary mask showing whether a pixel is inside of a polygon (of any type)   |
| Gridded Population of the World (CIESIN, 2017)                      | population_density                                    | Log transform then normalized with $\mu = 3.0$ and $\sigma = 1.0$ .  |
| NASADEM Digital Elevation (NASA JPL, 2020)                          | elevation   | Convert elevation to slope as the local gradient using the 4-connected neighbors, then converted to radians.                 |
| Oil Palm Plantation (Forest Data Partnership, 2025)                 | probability   | None   |
| CloudScore+ (Pasquarella et al., 2023)                              | cs  | None   |
| Global Roads Inventory Project (Meijer et al., 2018)                | roads   | Compute the distance to the nearest road in m, clipped at 5000, then divided by 5000.  |
| Global Mangrove Distribution (Simard et al., 2019)                  | agb   | None   |
| Global Wetland with Fine Classification System (Zhang et al., 2023) | b1  | Convert to binary mask indicating a non-zero value of any category   |

Table 3: Preprocessing applied to each data source.

Table 3 shows the preprocessing steps applied to each data source. For each data source, we applied preprocessing to bring values into (either roughly or exactly) having mean of 0 and standard deviation 1, except for binary layers which we left as (0, 1). Data sources with long-tailed values such as Sentinel-2 imagery and population were log-transformed.

For the Random Forest model, we first performed all of the preprocessing required for the deep learning models, then we composited the satellite image timeseries into a cloud-free mean as described in Table 3, and for a given pixel, we computed for each feature a vector consisting of the mean, standard deviation, variance, and each 10th-percentile over the  $63 \times 63$  patch centered on that pixel. To limit dataset size, we extracted patches centered on pixels arranged over a regular grid of spacing  $31 \times 31$ . This results in a dataset containing fewer pixels than the tile-based models, but this reflects the fundamental difference between the two approaches: tabular-style models like Decision Trees use features that are engineered to be informative about the phenomenon of interest, and thus typically carry more information (such as the median luminance of a patch of pixels) than the raw features used in deep learning models (such as the luminance of a single pixel).

### 3.3.2 HYPERPARAMETERS

| model         | parameters   |
|---------------|--|
| Random Forest | num trees = 20   |
| UNet3D        | feature dimension = 8  |
| U-TAE         | attention heads = 8<br>model dimension = 128<br>k = 16<br>encoder widths = [64, 64, 64, 128]<br>decoder widths = [32, 32, 64, 128] |
| TSViT         | head dimension = 64<br>num heads = 4<br>patch size = $4 \times 4$<br>spatial depth = 4<br>temporal depth = 4<br>width = 192        |

Table 4: Model and training hyperparameters.

Table 4 shows the model configuration parameters used for training each model.

All deep learning models were trained on Google TPUv3 with SGD with Nesterov acceleration Nesterov (1983); Sutskever et al. (2013) momentum of 0.9, gradient norm clipping of 1.0 Pascanu et al. (2012), and a cosine weight decay schedule Loshchilov & Hutter (2016).

For all models, we tuned hyperparameters using all data (satellite imagery, auxiliary layers, and change history) for the 2023 split, which has the most historical data and is closest in time to the present, so we would expect its dynamics to be most similar to today’s. For all deep learning models, we swept over learning rate, batch size, weight decay, gradient clipping norm, number of warm-up epochs, and total number of epochs, and we found that a learning rate of 0.3, batch size of 512, and weight decay of  $1.0 \times 10^{-4}$ , gradient clipping norm of 1.0, 1 warm-up epoch, and 16 total epochs were optimal (or among several equivalently optimal values).

We also compared binary cross entropy loss with several variants of Dice loss, but mainly Tanimoto Dice loss with complement (Diakogiannis et al., 2019) which we found to work the best among Dice loss variants. We swept over several ratios of weight between the two, ranging from fully cross entropy to fully Dice loss. We found that all models performed best with fully cross entropy loss.

Finally, for each model, we swept over model-specific parameters, finding the values listed in Table 4 to be optimal (or among several equivalently optimal values).



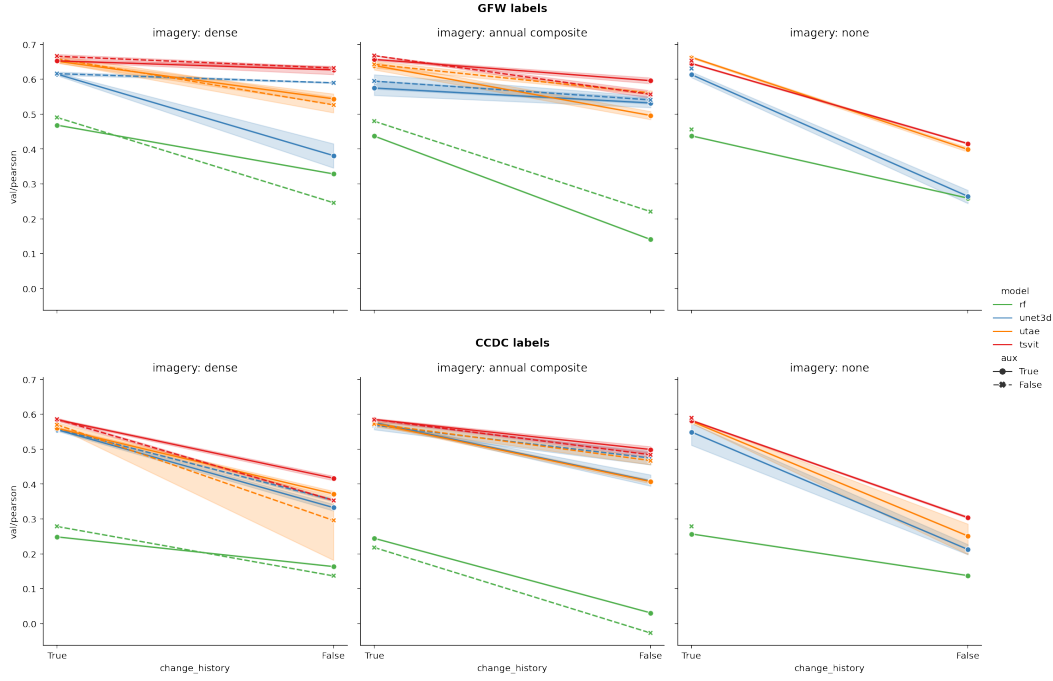


Figure 3: Tile-wise Pearson correlation for all ablation conditions, as a function of the presence/absence of the change-history layer (mean over 5 seeds, rounded to 2 decimal places, with shaded area showing the 95 confidence interval, except for the Random Forest (RF) model, whose training is deterministic).

For the Random Forest model, we used the default parameters for the YDF gradient-boosted learner model except with numerical discretization which dramatically speeds up training with minimal effect on accuracy. We swept over patch size, grid spacing, and the number of trees, and found that a patch size of 63, grid spacing of 32, and 20 trees performed best. In order to limit the number of features, we also composited the dense Sentinel-2 imagery by taking the mean over all time-steps after masking out pixels with less than a 0.6 CloudScore+ threshold.

## 4 RESULTS

We measured Area Under the ROC Curve (ROC-AUC) for per-pixel classification and Pearson correlation with the proportion of deforestation over an entire tile. ROC-AUC measures the tradeoff between false positives and false negatives as the decision threshold is varied. Tile-level Pearson correlation measures the linear relationship between the mean probability of deforestation over the entire tile compared to the proportion of pixels actually deforested. We found that ROC-AUC scores are very similar across models and across years, while tile-level Pearson correlation is more varied. This suggests that there may be a ceiling on how well any model can classify individual pixels (as measured by ROC-AUC), yet some models may be much better at broadly predicting the amount of deforestation in a given area (as measured by the tile-level correlation). This latter effect probably also accords better with downstream use-cases, as users will most likely care about deforestation patterns at scales much coarser than 30m. Therefore, in our analysis we only report tile-level Pearson correlation.

Importantly, we compute metrics for all pixels in a tile, in contrast to Ball et al. (2022), who computed metrics over only the single central pixel of each tile. Whole-tile metrics are important because performing inference (i.e. map-making) with deep learning models requires stitching together tiles rather than pixels, otherwise it would require an entire inference pass per pixel, which would be prohibitively slow and costly. For example, rendering a map that uses the central  $96 \times 96$  pixels of each tile would require nearly  $10,000 \times$  fewer inference passes than if we rendered pixel-by-pixel.

Therefore it is important that our metrics measure model performance in this context, reflecting how the models will actually be used in practice.

We aimed to compare the effectiveness of three classes of input features: imagery, auxiliary layers such as roads, protected areas, etc., and change history. For all models, we tested all valid combinations of these three sets of features. Figure 3 and Table A.1 show tile-level Pearson correlation for all ablation conditions.

We can observe several patterns from these results. First, the TSViT models performs the best on average. Second, the change history layer is important; removing it results in a decrease in performance in all cases. Third, change history alone is sufficient to achieve the best scores. Fourth, in many cases, removing the auxiliary layers actually improves performance. Fifth, using imagery with a longer temporal context, such as the GFC annual composites, results in models that are more robust to the absence of change history information. Lastly, the scores for CCDC-derived labels are lower than for GFC labels, probably reflecting the fact that the CCDC labels are noisier.

The observation that change history alone is sufficient for good performance is perhaps surprising, but this result underscores previous findings in the literature that the best predictor of future deforestation is proximity to previous deforestation (Rosa et al., 2013). However the change history layer also performs two other significant functions in our dataset. First, the change history provides more than just distance to recent deforestation for a target pixel, instead providing the full spatial and temporal history of deforestation in the whole tile, including for example local waves of deforestation – rich information that an expressive model like TSViT can be expected to learn to make use of. Second, the change history informs the model about the dynamics and state of the change detection algorithm itself. The models have to not only learn the (implicit) true dynamics of forest change, they also have to learn how those dynamics are captured and represented by the algorithm that generates the labels. Particularly, the change history allows the model to understand the “state” of the detection algorithm at the time of prediction, for example whether a particular pixel has already been classified as changed in a previous year, which we might expect to be highly useful for reducing noise and error in the predictions.

|             | 2019 | 2020 | 2021 | 2022 | 2023 |
|-------------|------|------|------|------|------|
| GFW labels  | 0.64 | 0.62 | 0.65 | 0.66 | 0.65 |
| CCDC labels | 0.57 | 0.62 | 0.51 | 0.61 | 0.58 |

Table 5: Tile-wise Pearson correlation for the TSViT model using GFC imagery plus change-history input features. Scores are the mean over 5 seeds (rounded to 2 decimal places).

Given that several configurations of model and data achieve similar results, a natural question is what setup is best for practical use? Given equal performance, smaller models are generally better, as they reduce computational cost and speed up training and inference. This would suggest the change-history-only variants are most desirable, however we observed that including some satellite imagery results moderately lessened tiling artifacts at inference time, therefore we suggest using the TSViT model with GFC imagery in practical situations. To further evaluate this combination, we trained a model on each of the 5 previous years. Results are shown in Table 5, where we can see that performance is similar for all 5 years.

Figure 4 shows several densely rendered risk forecast maps. These were generated by running inference over a regular grid of  $2.88\text{km} \times 2.88\text{km}$  (i.e. keeping the central  $96 \times 96$  30m pixels of each  $224 \times 224$  pixel image). We can see that even though the models that generated each forecast all achieve similar scores, they sometimes produce qualitatively different risk predictions. For example, the choice of ground truth labeling algorithm (GFW-GFC versus CCDC) significantly impacts the output. We can also see the risk predictions generated by the TSViT model tend to be more diffuse than those generated by the U-TAE model, and this also causes them to have more distinct tiling artifacts which occur at the borders between independent model forward passes. Lastly, we see that while the choice of input imagery has a qualitative effect, it is less than those induced by the label or model architecture. Based on these results, we advise that the choice of model be informed by the requirements of the particular use case, such as what spatial scale is most relevant, how com-

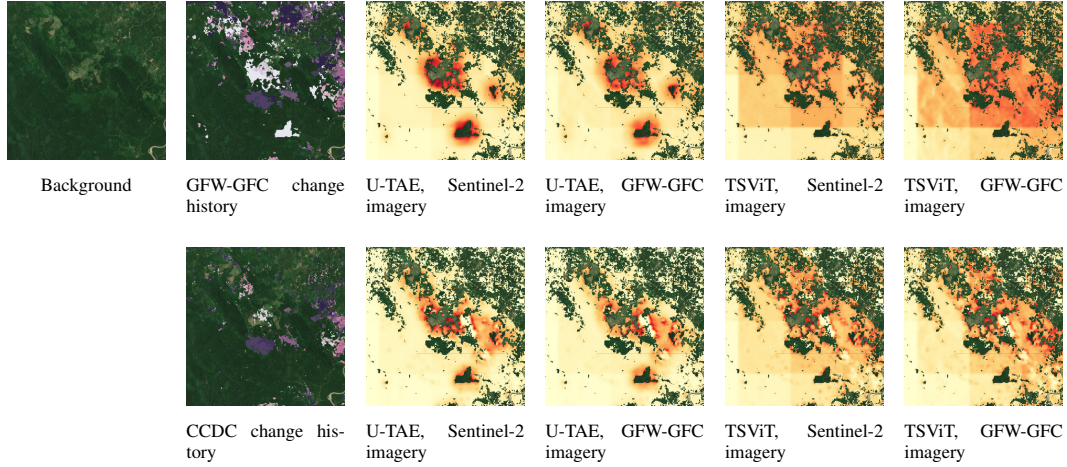


Figure 4: Each image shows a roughly  $9 \times 9$  km area in northeast Sumatra, Indonesia. The change history images show older change in dark purple progressing to newer change in light purple. The risk forecasts are for 2023, with previously deforested area (according to GFC) masked out (and thus showing the background imagery). Light yellow represents lower relative risk and red represents higher relative risk. The color scale has been slightly adjusted for each image so that they span similar color ranges. All models were trained with change history, but without auxiliary layers (which we observed to have minimal qualitative effect).

putationally efficient, and that models be evaluated with respect to the particular problem domain in question.

## 5 ETHICS

Deforestation prediction models aim to advance scientific understanding, protect biodiversity, enable proactive forest management, and inform global industry standards. As with any research, the responsible development and deployment of such models raises ethical and societal considerations. Here, we focus on two categories of pre-deployment considerations concretely associated with our model, namely, having to do with information *flattening*, as well as risks arising from potential model inaccuracies.

First, as proposed by Francès & Ricci (2020), relying primarily on remote sensing data risks a general *flattening* of knowledge and information, including in the context of deforestation. By relying on measurements conducted from space, there is the potential for losing critical pieces of local context, including important social, cultural, and political nuances that influence deforestation patterns. For instance, a model may accurately predict that rainforests managed by Indigenous peoples have low risk of deforestation without, however, reflecting that such a low risk is the result of those communities’ successful efforts at warding off deforestation (Sze et al., 2021). This means that even technically accurate, high-level prediction methods may lead to oversimplified understandings of complex local dynamics, in this instance potentially undermining the effectiveness of Indigenous Peoples’ conservation efforts. Similarly, failing to integrate deforestation risk with biodiversity indices might result in neglecting areas of high ecological importance, which underscores the need for a more holistic approach that combines deforestation risk assessments with comprehensive biodiversity data. It is particularly important to be aware of risks associated with information “flattening” if we consider that policy recommendations may be developed on the back of deforestation predictions.

A second category of ethical risks relates to potential mishandling of inevitable inaccurate predictions, i.e. false negatives and false positives. In this context, false negatives are cases where a model inaccurately predicts that a given area is not at risk of deforestation, potentially resulting in less protection or management of a genuinely at-risk area. Here, we can draw an analogy to fisheries prediction models, where recent evidence suggests that widespread overestimation of fish stocks may have contributed to systemic overfishing and, by extension, to global stock collapse (Edgar et al., 2024). Conversely, false positives, or cases where the model predicts high risk where it should

not be, may incur undue scrutiny or otherwise negatively affect landowners, particularly smallholders who may lack the capacity or economic influence to counter claims of deforestation risk.

While using deforestation predictions carries risk, we believe that these risks can be mitigated in several ways, with responsibility jointly falling across all stakeholders involved in producing, deploying, and using such forecasts. For researchers, it is important to not only make prediction models as accurate as possible, but to also characterize how well they perform and to what extent and in what situations they can be relied upon. For deployers, such as those who are hosting model outputs and providing data to users, open source and open access creates a level playing field for information access that allows all stakeholders from governments to commercial actors to NGOs to landowners to participate in risk-informed decisions. Finally, for users it is important that deforestation predictions are used as just one element of a more holistic, human-driven decision making process that is grounded on a range of evidence and contextual information, including but not limited to deforestation predictions, regardless of how accurate these may be.

## 6 DISCUSSION, LIMITATIONS, AND FUTURE WORK

We have presented the ForestCast dataset, the first dataset dedicated to training deep learning models for the task of deforestation risk prediction. Our study demonstrates that deep learning models can accurately forecast deforestation risk, and that they can even do so with only minimal data, namely a single layer summarizing the past history of forest change. It also reveals several limitations and avenues for refinement.

First, our results have revealed a pattern whereby longer temporal context correlates to better performance, with models trained on 20 year change history outperforming up to 10 years of annual composite satellite imagery, which in turn outperforms a single year of dense satellite image time-series. This is true even when that context is represented in a relatively compressed form (e.g. a single change history image versus a rich imagery). Future work should try to assess how much temporal context is sufficient and to further disentangle the relative effect of input feature richness versus temporal context.

Second, despite leveraging an extensive historical record of satellite imagery, our analysis is inherently constrained by data availability and quality. One avenue for enriching the input features may be by incorporating recently developed "foundation" models that compress or embed large multi-modal Earth observation data into compact, learned representations (Zhu et al., 2024; Brown et al., 2025). However, even those models cannot account for crucial predictive factors such as political and legal frameworks, which remain inaccessible through remote sensing. Furthermore, the accuracy of our predictions is contingent upon the quality of the ground-truth data, which, in our case, is algorithmically generated. Consequently, the curation and accuracy of deforestation labels represents a significant opportunity for improvement. Towards this end, recent improvements in delineating natural forests from other types of forest (Neumann et al., 2025) and understanding the drivers of deforestation (Sims et al., 2025) seem promising.

Related to data is the fact that deforestation is a dynamic, non-stationary process, where the relationship between predictive variables and deforestation patterns evolves over time due to factors like political shifts, regulatory changes, and societal attitudes. Future research should explore the integration of temporal data reflecting these variables, alongside the spatial features traditionally used in such studies.

Additionally, the practical implications of current evaluation metrics for real-world applications remain unclear. While achieving high accuracy is a natural objective, the specific methodologies employed to measure accuracy can yield varying interpretations and may not fully align with the needs of downstream users.

Lastly, to make deforestation risk models truly useful, they must be reliable and trustworthy. As discussed in Section 5, beyond mere accuracy, these models should characterize when, where, and how accurate they are. Incorporating calibrated uncertainty estimates and explainability techniques are promising directions for future exploration, that would enhance the transparency and utility of these models.

## REFERENCES

- James G C Ball, Katerina Petrova, David A Coomes, and Seth Flaxman. Using deep convolutional neural networks to forecast spatial patterns of amazonian deforestation. *Methods Ecol. Evol.*, 13(11):2622–2634, November 2022. ISSN 2041-210X. doi: 10.1111/2041-210X.13953. URL <https://besjournals.onlinelibrary.wiley.com/doi/10.1111/2041-210X.13953>.
- Nikolaos Ioannis Bountos, Arthur Ouaknine, and David Rolnick. FoMo-bench: a multi-modal, multi-scale and multi-task forest monitoring benchmark for remote sensing foundation models. *arXiv [cs.CV]*, 15 December 2023. URL <http://arxiv.org/abs/2312.10114>.
- Christopher F Brown, Michal R Kazmierski, Valerie J Pasquarella, William J Rucklidge, Masha Samsikova, Chenhui Zhang, Evan Shelhamer, Estefania Lahera, Olivia Wiles, Simon Ilyushchenko, Noel Gorelick, Lihui Lydia Zhang, Sophia Alj, Emily Schechter, Sean Askay, Oliver Guinan, Rebecca Moore, Alexis Boukouvalas, and Pushmeet Kohli. AlphaEarth foundations: An embedding field model for accurate and efficient global mapping from sparse label data. *arXiv [cs.CV]*, 8 September 2025. doi: 10.48550/arXiv.2507.22291. URL <http://arxiv.org/abs/2507.22291>.
- CIESIN. Gridded population of the world, version 4 (gpwv4): Population density, revision 11, 2017. URL <http://dx.doi.org/10.7927/H49C6VHW>.
- Copernicus. Sentinel data, 2025.
- Gretchen C Daily, Susan Alexander, Paul R Ehrlich, Larry Goulder, Jane Lubchenco, Pamela A Matson, Harold A Mooney, Sandra Postel, Stephen H Schneider, David Tilman, and George M Woodwell. Benefits supplied to human societies by natural ecosystems. *Issues Ecol.*, (2), 1997. ISSN 1092-8987. URL <https://www.esa.org/wp-content/uploads/2013/03/issue2.pdf>.
- Foivos I Diakogiannis, François Waldner, Peter Caccetta, and Chen Wu. ResUNet-a: a deep learning framework for semantic segmentation of remotely sensed data. *arXiv [cs.CV]*, 1 April 2019. URL <http://arxiv.org/abs/1904.00592>.
- Alexey Dosovitskiy, Lucas Beyer, Alexander Kolesnikov, Dirk Weissenborn, Xiaohua Zhai, Thomas Unterthiner, Mostafa Dehghani, Matthias Minderer, Georg Heigold, Sylvain Gelly, Jakob Uszkoreit, and Neil Houlsby. An image is worth 16x16 words: Transformers for image recognition at scale. *arXiv [cs.CV]*, 22 October 2020. URL <http://arxiv.org/abs/2010.11929>.
- J R Eastman and J Toledano. A short presentation of the land change modeler (LCM). In *Geomatic Approaches for Modeling Land Change Scenarios*, Lecture notes in geoinformation and cartography, pp. 499–505. Springer International Publishing, Cham, 2018. ISBN 9783319608006, 9783319608013. doi: 10.1007/978-3-319-60801-3\_36. URL [https://scholar.google.com/citations?view\\_op=view\\_citation&hl=en&citation\\_for\\_view=JrGeWbYAAAAJ:K3LRdlH-MEOC](https://scholar.google.com/citations?view_op=view_citation&hl=en&citation_for_view=JrGeWbYAAAAJ:K3LRdlH-MEOC).
- Graham J Edgar, Amanda E Bates, Nils C Krueck, Susan C Baker, Rick D Stuart-Smith, and Christopher J Brown. Stock assessment models overstate sustainability of the world’s fisheries. *Science*, 385(6711):860–865, 23 August 2024. ISSN 0036-8075, 1095-9203. doi: 10.1126/science.adl6282. URL <https://www.science.org/doi/10.1126/science.adl6282>.
- Tim Engelmann and Malte Toetzke. Can deep learning help to forecast deforestation in the amazonian rainforest? In *NeurIPS 2023 Workshop on Tackling Climate Change with Machine Learning*. Climate Change AI, 16 December 2023. URL <https://www.climatechange.ai/papers/neurips2023/22/paper.pdf>.
- European Commission: Directorate-General for Environment. *EU Deforestation Regulation – An opportunity for smallholder*. Publications Office of the European Union, 2023. doi: 10.2779/9252. URL <https://data.europa.eu/doi/10.2779/9252>.

European Union. Regulation (EU) 2023/1115 of the European Parliament and of the Council of 31 May 2023 on the making available on the Union market and the export from the Union of certain commodities and products associated with deforestation and forest degradation and repealing Regulation (EU) No 995/2010. Official Journal of the European Union, June 2023. URL <https://eur-lex.europa.eu/legal-content/EN/TXT/?uri=CELEX:32023R1115>. Accessed: Dec 2024.

Food and Agriculture Organization. *The state of the world's forests 2014: enhancing the socio-economic benefits from forests*. Food & Agriculture Organization of the United Nations (FAO), Rome, Italy, 30 November 2014. ISBN 9789251082690. URL <https://openknowledge.fao.org/handle/20.500.14283/i3710e>.

Forest Data Partnership. Palm probability model (community models), 2025.

Diana Franc s and Noemi Ricci. Ethical advisory report AN EARLY WARNING SYSTEM FOR EARLY DETECTION AND PREDICTING DEFORESTATION. Technical report, 1 April 2020. URL [https://www.researchgate.net/publication/350354148\\_Ethical\\_Advisory\\_Report\\_AN\\_EARLY\\_WARNING\\_SYSTEM\\_FOR\\_EARLY\\_DETECTION\\_AND\\_PREDICTING\\_DEFORESTATION\\_Ethical\\_Advisory\\_Report\\_WWF\\_Netherlands](https://www.researchgate.net/publication/350354148_Ethical_Advisory_Report_AN_EARLY_WARNING_SYSTEM_FOR_EARLY_DETECTION_AND_PREDICTING_DEFORESTATION_Ethical_Advisory_Report_WWF_Netherlands).

Vivien Sainte Fare Garnot and Loic Landrieu. Lightweight temporal self-attention for classifying satellite image time series. *arXiv [cs.CV]*, 1 July 2020. URL <http://arxiv.org/abs/2007.00586>.

Vivien Sainte Fare Garnot and Loic Landrieu. Panoptic segmentation of satellite image time series with convolutional temporal attention networks. *arXiv [cs.CV]*, 16 July 2021. URL <http://arxiv.org/abs/2107.07933>.

Elizabeth Goldman, Nancy Harris, and Thomas Maschler. Predicting future forest loss in the democratic republic of the congo's carpe landscapes. [https://files.wri.org/d8/s3fs-public/predicting-future-forest-loss-democratic-republic-congos-carpe-landscapes\\_0.pdf](https://files.wri.org/d8/s3fs-public/predicting-future-forest-loss-democratic-republic-congos-carpe-landscapes_0.pdf). Accessed: 2022-9-1.

Noel Gorelick, Matt Hancher, Mike Dixon, Simon Ilyushchenko, David Thau, and Rebecca Moore. Google earth engine: Planetary-scale geospatial analysis for everyone. *Remote Sensing of Environment*, 2017. doi: 10.1016/j.rse.2017.06.031. URL <https://doi.org/10.1016/j.rse.2017.06.031>.

Noel Gorelick, Zhiqiang Yang, Paulo Ar valo, Eric L Bullock, Katherin Patricia Insfr n, and Sean P Healey. A global time series dataset to facilitate forest greenhouse gas reporting. *Environ. Res. Lett.*, 18(8):084001, 1 August 2023. ISSN 1748-9326. doi: 10.1088/1748-9326/ace2da. URL <https://iopscience.iop.org/article/10.1088/1748-9326/ace2da/meta>.

Mathieu Guilleme-Bert, Sebastian Bruch, Richard Stotz, and Jan Pfeifer. Yggdrasil decision forests: A fast and extensible decision forests library. In *Proceedings of the 29th ACM SIGKDD Conference on Knowledge Discovery and Data Mining, KDD 2023, Long Beach, CA, USA, August 6-10, 2023*, pp. 4068–4077, 2023. doi: 10.1145/3580305.3599933. URL <https://doi.org/10.1145/3580305.3599933>.

M C Hansen, P V Potapov, R Moore, M Hancher, S A Turubanova, A Tyukavina, D Thau, S V Stehman, S J Goetz, T R Loveland, A Kommareddy, A Egorov, L Chini, C O Justice, and J R G Townshend. High-resolution global maps of 21st-century forest cover change. *Science*, 342(6160):850–853, 15 November 2013. ISSN 0036-8075,1095-9203. doi: 10.1126/science.1244693. URL <http://dx.doi.org/10.1126/science.1244693>.

Michael Holder. BlackRock steps up investor pressure on its portfolio polluters. <https://trellis.net/article/blackrock-steps-investor-pressure-its-portfolio-polluters/>, 24 February 2021. Accessed: 2024-12-.

- IPBES. Global assessment report on biodiversity and ecosystem services of the intergovernmental science-policy platform on biodiversity and ecosystem services, 2019. URL <https://zenodo.org/records/6417333>.
- Rodolfo Jaffé, Samia Nunes, Jorge Filipe Dos Santos, Markus Gastauer, Tereza C Giannini, Wilson Nascimento, Jr, Marcio Sales, Carlos M Souza, Pedro W Souza-Filho, and Robert J Fletcher. Forecasting deforestation in the brazilian amazon to prioritize conservation efforts. *Environ. Res. Lett.*, 16(8):084034, 29 July 2021. ISSN 1748-9326. doi: 10.1088/1748-9326/ac146a. URL <https://iopscience.iop.org/article/10.1088/1748-9326/ac146a/meta>.
- Alexandre Lacoste, Nils Lehmann, Pau Rodriguez, Evan David Sherwin, Hannah Kerner, Björn Lütjens, Jeremy Andrew Irvin, David Dao, Hamed Alemohammad, Alexandre Drouin, Mehmet Gunturkun, Gabriel Huang, David Vazquez, Dava Newman, Yoshua Bengio, Stefano Ermon, and Xiao Xiang Zhu. GEO-bench: Toward foundation models for earth monitoring. *arXiv [cs.LG]*, 6 June 2023. URL <http://arxiv.org/abs/2306.03831>.
- Ilya Loshchilov and Frank Hutter. SGDR: Stochastic gradient descent with warm restarts. *arXiv [cs.LG]*, 13 August 2016. doi: 10.48550/arXiv.1608.03983. URL <http://arxiv.org/abs/1608.03983>.
- Johan R Meijer, Mark A J Huijbregts, Kees C G J Schotten, and Aafke M Schipper. Global patterns of current and future road infrastructure. *Environ. Res. Lett.*, 13(6):064006, 1 June 2018. ISSN 1748-9326. doi: 10.1088/1748-9326/aabd42. URL <http://dx.doi.org/10.1088/1748-9326/aabd42>.
- NASA JPL. NASADEM merged DEM global 1 arc second, 2020. URL [http://dx.doi.org/10.5067/MEaSURES/NASADEM/NASADEM\\_HGT.001](http://dx.doi.org/10.5067/MEaSURES/NASADEM/NASADEM_HGT.001).
- National Institute For Space Research. Deforestation – legal amazon. URL <https://terrabrasilis.dpi.inpe.br/downloads/>.
- Yu. Nesterov. A method for unconstrained convex minimization problem with the rate of convergence  $O(1/k^2)$ . *Doklady Akademii Nauk Sssr*, 269(3):543–547, 1983.
- Maxim Neumann, Anton Raichuk, Radost Stanimirova, Michelle Sims, Sarah Carter, Elizabeth Goldman, Melanie Rey, Yuchang Jiang, Keith Anderson, Petra Poklukar, Katelyn Tarrio, Myroslava Lesiv, Steffen Fritz, Nicholas Clinton, Charlotte Stanton, Dan Morris, and Drew Purves. Natural forests of the world - a 2020 baseline for deforestation and degradation monitoring. <https://eartharxiv.org/repository/view/9085/>, 29 April 2025. Accessed: 2025-10-30.
- Razvan Pascanu, Tomas Mikolov, and Yoshua Bengio. On the difficulty of training recurrent neural networks. *arXiv [cs.LG]*, 21 November 2012. doi: 10.48550/arXiv.1211.5063. URL <http://arxiv.org/abs/1211.5063>.
- Valerie J Pasquarella, Christopher F Brown, Wanda Czerwinski, and W Rucklidge. Comprehensive quality assessment of optical satellite imagery using weakly supervised video learning. *2023 IEEE/CVF Conference on Computer Vision and Pattern Recognition Workshops (CVPRW)*, pp. 2125–2135, 1 June 2023. doi: 10.1109/CVPRW59228.2023.00206. URL [https://openaccess.thecvf.com/content/CVPR2023W/EarthVision/papers/Pasquarella\\_Comprehensive\\_Quality\\_Assessment\\_of\\_Optical\\_Satellite\\_Imagery\\_Using\\_Weakly\\_Supervised\\_CVPRW\\_2023\\_paper.pdf](https://openaccess.thecvf.com/content/CVPR2023W/EarthVision/papers/Pasquarella_Comprehensive_Quality_Assessment_of_Optical_Satellite_Imagery_Using_Weakly_Supervised_CVPRW_2023_paper.pdf).
- Olaf Ronneberger, Philipp Fischer, and Thomas Brox. U-net: Convolutional networks for biomedical image segmentation. In Nassir Navab, Joachim Hornegger, William M Wells, and Alejandro F Frangi (eds.), *Medical Image Computing and Computer-Assisted Intervention – MICCAI 2015*, pp. 234–241, Cham, 2015. Springer International Publishing. ISBN 9783319245744.
- Isabel M D Rosa, Drew Purves, Carlos Souza, Jr, and Robert M Ewers. Predictive modelling of contagious deforestation in the brazilian amazon. *PLoS One*, 8(10):e77231, 18 October 2013. ISSN 1932-6203. doi: 10.1371/journal.pone.0077231. URL <http://dx.doi.org/10.1371/journal.pone.0077231>.

- Samapriya Roy, Tyson Swetnam, and Andrew Saah. Samapriya/awesome-gee-community-datasets: Community catalog, 2024. URL <https://zenodo.org/records/14042069>.
- Rose Rustowicz, Robin Cheong, Lijing Wang, Stefano Ermon, M Burke, and D Lobell. Semantic segmentation of crop type in africa: A novel dataset and analysis of deep learning methods. In *Proceedings of the IEEE/CVF Conference on Computer Vision and Pattern Recognition (CVPR) Workshops*, pp. 75–82, 2019. URL [https://openaccess.thecvf.com/content\\_CVPRW\\_2019/html/cv4gc/Rustowicz\\_Semantic\\_Segmentation\\_of\\_Crop\\_Type\\_in\\_Africa\\_A\\_Novel\\_Dataset\\_CVPRW\\_2019\\_paper.html](https://openaccess.thecvf.com/content_CVPRW_2019/html/cv4gc/Rustowicz_Semantic_Segmentation_of_Crop_Type_in_Africa_A_Novel_Dataset_CVPRW_2019_paper.html).
- Marcio Sales, Sytze de Bruin, Martin Herold, Phaeton Kyriakidis, and Carlos Souza, Jr. A spatiotemporal geostatistical hurdle model approach for short-term deforestation prediction. *Spatial Statistics*, 21:304–318, 1 August 2017. ISSN 2211-6753. doi: 10.1016/j.spasta.2017.06.003. URL <https://www.sciencedirect.com/science/article/pii/S221167531730163X>.
- Satelligence. Scaling the forest loss risk index (FLRI) approach across landscapes. Technical report, 23 May 2022. URL <https://satelligence.com/wp-content/uploads/2024/02/FLRI-olam.pdf>.
- Tarek Sboui, Salwa Saidi, and Ahmed Lakti. A machine-learning-based approach to predict deforestation related to oil palm: Conceptual framework and experimental evaluation. *Appl. Sci. (Basel)*, 13(3):1772, 30 January 2023. ISSN 2076-3417,2076-3417. doi: 10.3390/app13031772. URL <https://www.mdpi.com/2076-3417/13/3/1772>.
- André Schröder. European bill passes to ban imports of deforestation-linked commodities. <https://news.mongabay.com/2022/09/european-bill-passes-to-ban-imports-of-deforestation-linked-commodities/>, 15 September 2022. Accessed: 2024-12-.
- M Simard, L Fatoyinbo, C Smetanka, V H Rivera-monroy, E Castañeda-Moya, N Thomas, and T Van der stocken. Global mangrove distribution, aboveground biomass, and canopy height, 2 May 2019. URL <http://dx.doi.org/10.3334/ORNLDAAAC/1665>.
- Michelle J Sims, Radost Stanimirova, Anton Raichuk, Maxim Neumann, Jessica Richter, Forrest Follett, James MacCarthy, Kristine Lister, Christopher Randle, Lindsey Sloat, Elena Esipova, Jaelah Jupiter, Charlotte Stanton, Dan Morris, Christy Melhart Slay, Drew Purves, and Nancy Harris. Global drivers of forest loss at 1 km resolution. *Environ. Res. Lett.*, 20(7):074027, 1 July 2025. ISSN 1748-9326. doi: 10.1088/1748-9326/add606. URL <http://dx.doi.org/10.1088/1748-9326/add606>.
- Carlos M Souza, Jr, Julia Z. Shimbo, Marcos R Rosa, Leandro L Parente, Ane A. Alencar, Bernardo F T Rudorff, Heinrich Hasenack, Marcelo Matsumoto, Laerte G. Ferreira, Pedro W M Souza-Filho, Sergio W de Oliveira, Washington F Rocha, Antônio V Fonseca, Camila B Marques, Cesar G Diniz, Diego Costa, Dyeden Monteiro, Eduardo R Rosa, Eduardo Vélez-Martin, Eliseu J Weber, Felipe E B Lenti, Fernando F Paternost, Frans G C Pareyn, João V Siqueira, José L Viera, Luiz C Ferreira Neto, Marciano M Saraiva, Marcio H Sales, Moises P G Salgado, Rodrigo Vasconcelos, Soltan Galano, Vinicius V Mesquita, and Tasso Azevedo. Reconstructing three decades of land use and land cover changes in brazilian biomes with landsat archive and earth engine. *Remote Sens. (Basel)*, 12(17):2735, 25 August 2020. ISSN 2072-4292,2072-4292. doi: 10.3390/rs12172735. URL <https://www.mdpi.com/2072-4292/12/17/2735>.
- Ilya Sutskever, James Martens, George E Dahl, and Geoffrey E Hinton. On the importance of initialization and momentum in deep learning. In *International conference on machine learning*, pp. 1139–1147, 2013.
- Jocelyne S Sze, L Roman Carrasco, Dylan Childs, and David P Edwards. Reduced deforestation and degradation in indigenous lands pan-tropically. *Nat. Sustain.*, 5(2):123–130, 25 November 2021. ISSN 2398-9629,2398-9629. doi: 10.1038/s41893-021-00815-2. URL <https://www.nature.com/articles/s41893-021-00815-2>.



- Michail Tarasiou, Erik Chavez, and Stefanos Zafeiriou. ViTs for SITS: Vision transformers for satellite image time series. *arXiv [cs.CV]*, 12 January 2023. URL <http://arxiv.org/abs/2301.04944>.
- UNEP-WCMC and IUCN. Protected planet: The world database on protected areas (WDPA), 2024. URL [www.protectedplanet.net](http://www.protectedplanet.net).
- Anouk van Stokkom, Jorn Dallinga, Michael Debuyser, Dirk Hoekman, Boris Kooij, Pablo Pacheco, David Thau, Suzanne Valkman, and Hans Beukeboom. An innovative early warning system to tackle illegal deforestation. In *FIG Working Week*, 2020. URL [https://www.fig.net/resources/proceedings/fig\\_proceedings/fig2020/papers/ts06i/TS06I\\_van\\_stokkom\\_dallinga\\_10667.pdf](https://www.fig.net/resources/proceedings/fig_proceedings/fig2020/papers/ts06i/TS06I_van_stokkom_dallinga_10667.pdf).
- C Vancutsem, F Achard, J-F Pekel, G Vieilledent, S Carboni, D Simonetti, J Gallego, L E O C Aragão, and R Nasi. Long-term (1990-2019) monitoring of forest cover changes in the humid tropics. *Sci Adv*, 7(10), March 2021. ISSN 2375-2548. doi: 10.1126/sciadv.abe1603. URL <http://dx.doi.org/10.1126/sciadv.abe1603>.
- Ghislain Vieilledent, Christelle Vancutsem, Clément Bourgoïn, Pierre Ploton, Philippe Verley, and Frédéric Achard. Spatial scenario of tropical deforestation and carbon emissions for the 21st century. *bioRxiv*, pp. 2022.03.22.485306, 12 May 2023. doi: 10.1101/2022.03.22.485306. URL <https://www.biorxiv.org/content/10.1101/2022.03.22.485306v3>.
- Mikaela Weisse, Elizabeth Goldman, and Sarah Carter. Tropical forest loss drops steeply in brazil and colombia, but high rates persist overall. <https://research.wri.org/gfr/latest-analysis-deforestation-trends>, 4 April 2024. Accessed: 2024-12-.
- Xiao Zhang, Liangyun Liu, Tingting Zhao, Xidong Chen, Shangrong Lin, Jinqing Wang, Jun Mi, and Wendi Liu. GWL\_FCS30: a global 30 m wetland map with a fine classification system using multi-sourced and time-series remote sensing imagery in 2020. *Earth Syst. Sci. Data*, 15(1): 265–293, 17 January 2023. ISSN 1866-3508,1866-3516. doi: 10.5194/essd-15-265-2023. URL <https://doi.org/10.5194/essd-15-265-2023>.
- Xiao Xiang Zhu, Zhitong Xiong, Yi Wang, Adam J Stewart, Konrad Heidler, Yuanyuan Wang, Zhenghang Yuan, Thomas Dujardin, Qingsong Xu, and Yilei Shi. On the foundations of earth and climate foundation models. *arXiv [cs.AI]*, 7 May 2024. doi: 10.48550/arXiv.2405.04285. URL <http://arxiv.org/abs/2405.04285>.
- Zhe Zhu and Curtis E Woodcock. Continuous change detection and classification of land cover using all available landsat data. *Remote Sens. Environ.*, 144:152–171, 25 March 2014. ISSN 0034-4257. doi: 10.1016/j.rse.2014.01.011. URL <https://www.sciencedirect.com/science/article/pii/S0034425714000248>.

## APPENDIX A RESULTS

|              |         |       |                | RF    | U-Net3D | U-TAE | TSViT |
|--------------|---------|-------|----------------|-------|---------|-------|-------|
| label source | imagery | aux   | change history |       |         |       |       |
| ccdc         | dense   | False | False          | 0.14  | 0.35    | 0.30  | 0.35  |
|              |         |       | True           | 0.28  | 0.56    | 0.57  | 0.59  |
|              |         | True  | False          | 0.16  | 0.33    | 0.37  | 0.42  |
|              |         |       | True           | 0.25  | 0.56    | 0.56  | 0.58  |
|              | annual  | False | False          | -0.03 | 0.47    | 0.47  | 0.48  |
|              |         |       | True           | 0.22  | 0.57    | 0.57  | 0.59  |
|              |         | True  | False          | 0.03  | 0.41    | 0.41  | 0.50  |
|              |         |       | True           | 0.24  | 0.58    | 0.57  | 0.59  |
|              | none    | False | True           | 0.28  | 0.58    | 0.58  | 0.59  |
|              |         |       | False          | 0.14  | 0.21    | 0.25  | 0.30  |
|              |         | True  | True           | 0.26  | 0.55    | 0.58  | 0.58  |
|              |         |       | False          | 0.26  | 0.55    | 0.58  | 0.58  |
| gfw          | dense   | False | False          | 0.25  | 0.59    | 0.53  | 0.63  |
|              |         |       | True           | 0.49  | 0.62    | 0.66  | 0.67  |
|              |         | True  | False          | 0.33  | 0.38    | 0.54  | 0.63  |
|              |         |       | True           | 0.47  | 0.61    | 0.65  | 0.65  |
|              | annual  | False | False          | 0.22  | 0.54    | 0.56  | 0.56  |
|              |         |       | True           | 0.48  | 0.59    | 0.64  | 0.67  |
|              |         | True  | False          | 0.14  | 0.53    | 0.50  | 0.60  |
|              |         |       | True           | 0.44  | 0.57    | 0.64  | 0.66  |
|              | none    | False | True           | 0.46  | 0.63    | 0.66  | 0.65  |
|              |         |       | False          | 0.26  | 0.26    | 0.40  | 0.42  |
|              |         | True  | True           | 0.44  | 0.61    | 0.66  | 0.65  |
|              |         |       | False          | 0.26  | 0.26    | 0.40  | 0.42  |

Table A.1: Tile-wise Pearson correlation for all ablation conditions (mean over 5 seeds, rounded to 2 decimal places, except for the Random Forest (RF) model, whose training is deterministic).

|              |           |       |                | RF   | U-Net3D | U-TAE | TSViT |
|--------------|-----------|-------|----------------|------|---------|-------|-------|
| label source | imagery   | aux   | change history |      |         |       |       |
| dense        | sentinel2 | False | False          | 0.74 | 0.72    | 0.75  | 0.73  |
|              |           |       | True           | 0.82 | 0.86    | 0.90  | 0.85  |
|              |           | True  | False          | 0.76 | 0.69    | 0.74  | 0.75  |
|              |           |       | True           | 0.83 | 0.86    | 0.90  | 0.85  |
|              | annual    | False | False          | 0.74 | 0.74    | 0.77  | 0.78  |
|              |           |       | True           | 0.83 | 0.86    | 0.90  | 0.85  |
|              |           | True  | False          | 0.76 | 0.71    | 0.76  | 0.79  |
|              |           |       | True           | 0.83 | 0.86    | 0.90  | 0.85  |
|              | none      | False | True           | 0.83 | 0.86    | 0.90  | 0.84  |
|              |           |       | False          | 0.72 | 0.61    | 0.67  | 0.66  |
|              |           | True  | True           | 0.83 | 0.85    | 0.90  | 0.85  |
|              |           |       | False          | 0.83 | 0.85    | 0.90  | 0.85  |
| gfw          | sentinel2 | False | False          | 0.80 | 0.82    | 0.85  | 0.86  |
|              |           |       | True           | 0.88 | 0.84    | 0.88  | 0.84  |
|              |           | True  | False          | 0.83 | 0.77    | 0.85  | 0.86  |
|              |           |       | True           | 0.88 | 0.84    | 0.89  | 0.84  |
|              | gfc       | False | False          | 0.80 | 0.81    | 0.85  | 0.86  |
|              |           |       | True           | 0.88 | 0.82    | 0.89  | 0.84  |
|              |           | True  | False          | 0.81 | 0.81    | 0.82  | 0.86  |
|              |           |       | True           | 0.88 | 0.82    | 0.89  | 0.84  |
|              | none      | False | False          | 0.88 | 0.84    | 0.89  | 0.83  |
|              |           |       | True           | 0.78 | 0.69    | 0.76  | 0.74  |
|              |           | True  | True           | 0.88 | 0.84    | 0.89  | 0.83  |
|              |           |       | False          | 0.88 | 0.84    | 0.89  | 0.83  |

Table A.2: Area under the ROC curve for all ablation conditions (mean over 5 seeds, rounded to 2 decimal places, except for the Random Forest (RF) model, whose training is deterministic).